NASA TECHNICAL NOTE

NASA TN D-3301

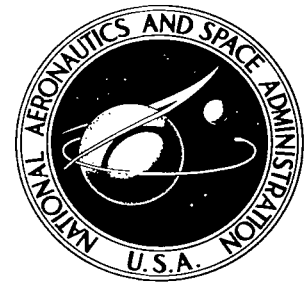

NASA TN D-3301

EXPERIMENTAL FLUTTER RESULTS FOR CORRUGATION-STIFFENED AND UNSTIFFENED PANELS

by Deene J. Weidman

Langley Research Center
Langley Station, Hampton, Va.

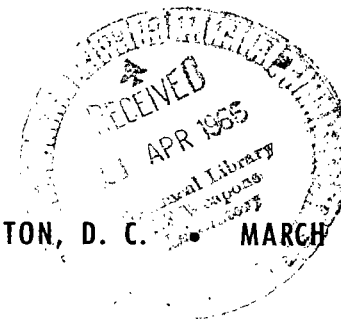

NATIONAL AERONAUTICS AND SPACE ADMINISTRATION • WASHINGTON, D. C. • MARCH 1966

ERRATA

NASA Technical Note D-3301

EXPERIMENTAL FLUTTER RESULTS FOR CORRUGATION-STIFFENED AND UNSTIFFENED PANELS

By Deene J. Weidman

March 1966

Errors in the stiffness ratios D_x/D_s presented in table I require corrections to this report as follows:

Page 12: Replace figure 7 with revised figure 7 attached.

Page 29: Correct values of D_x/D_s in the next-to-last column of table I as follows:

Panel	D_x/D_s
Free-edge panels	
U-1	3.024
U-2	2.743
V-1	2.303
V-2	3.416
V-3	3.416
V-4	2.872
V-5	2.872
V-6	2.520
H-1	2.487
Crushed-edge panels	
S-1	3.580
S-2	3.692
S-3	3.911
S-4	4.145
S-5	3.165
S-6	3.165
S-7	3.580
S-8	2.925
S-9	2.925
S-10	2.922

Completed 10 Jan 68
Lab

NASA-Langley, 1967

Issued 12-4-67

NASA TN D-3301

EXPERIMENTAL FLUTTER RESULTS FOR CORRUGATION-STIFFENED AND UNSTIFFENED PANELS

By Deene J. Weidman

Langley Research Center
Langley Station, Hampton, Va.

NATIONAL AERONAUTICS AND SPACE ADMINISTRATION

For sale by the Clearinghouse for Federal Scientific and Technical Information
Springfield, Virginia 22151 – Price $0.50

EXPERIMENTAL FLUTTER RESULTS FOR CORRUGATION-STIFFENED AND UNSTIFFENED PANELS

By Deene J. Weidman
Langley Research Center

SUMMARY

The results of a flutter investigation of 19 corrugation-stiffened and 6 flat unstiffened rectangular panels are presented. These results show that boundary conditions in the cross-stream direction have an important effect on panel flutter. It is also shown that the flutter of square orthotropic panels is not easily predicted, and that, at present, a flutter envelope appears to be the best available means for the prediction of the flutter boundaries for such panels. In addition, a method for analyzing the stiffness of corrugation-stiffened skin panels is presented. A "preflutter" solution is shown to approximate accurately the exact solution for simply supported panels with in-plane tension loads, but both solutions differ considerably from the experimental results.

INTRODUCTION

With the increased speed and performance of high-speed aircraft and missiles, the problem of flutter of the individual skin panels of such vehicles has become more pronounced and, indeed, has even governed design in some cases. Many skin panels of these vehicles are constructed of an exterior sheet stiffened by means of a single corrugated stiffening sheet attached directly to the skin. These panels are termed "corrugation-stiffened" panels herein. In the theoretical investigation of panel flutter, several basic approaches have long been available (see refs. 1 to 3), and recent extensions of these analyses (refs. 4 to 7) indicate a continuing interest in this problem. Experimental results, however, differ considerably from most analytical results particularly for corrugation-stiffened panels (see, for example, ref. 8), and the design of panels has, to a large extent, been accomplished with the use of an experimental flutter envelope such as is presented in reference 9.

In view of the difficulty in theoretically determining the flutter characteristics of corrugation-stiffened panels, it appears that experimental flutter data should be used to determine a flutter envelope for panel design until a proper analytical approach can be determined. Isotropic plate theory has been extended to orthotropic plates (if the orthotropic stiffnesses are known) as in references 8 and 9; but the validity of such an

extension is questioned in reference 10. However, this extension defines parameters that allow the experimental results to be compared in a logical manner; these parameters are used herein. The orthotropic stiffnesses of these corrugation-stiffened panels are calculated by the method shown in appendix A.

In this report, the results of a flutter investigation of both isotropic and corrugation-stiffened panels are presented. In the tests of corrugation-stiffened panels, both aerodynamic and panel stiffness factors were varied, as well as the boundary conditions on the ends of the corrugations. In all tests reported herein, the axis of the corrugations was always perpendicular to the direction of airflow, so that the boundary conditions on the ends of the corrugations are termed "cross-flow" boundary conditions. The pressure differential (difference between the cavity pressure and the free-stream pressure) was also varied for these panels. In the tests of isotropic panels, the aerodynamic parameters and pressure differential were varied, as well as the length-width ratio and thickness of the panel.

The experimental results are compared with the empirical flutter envelope from reference 9 and with the "exact" preflutter solution in which the exact eigenvalue equation for the simply supported case is solved for a conservative critical flutter value. This preflutter solution is compared with the exact solution and shown to be very accurate. A typical flutter boundary for free-edge panels from reference 5 is also presented. The experimental data, however, differ considerably from these solutions, and these differences are discussed.

SYMBOLS

The units used for the physical quantities in this paper are given both in the U.S. Customary Units and in the International System of Units (SI). Factors relating the two systems are given in reference 11, and those used in the present investigation are presented in appendix B.

$$A = \frac{N_x a^2}{D_x} - 2n^2\pi^2 \frac{a^2}{b^2}\frac{D_{xy}}{D_x}$$

A_O dimensionless enclosed area within a corrugation cell (see eq. (A8))

a,b length and width, respectively, of each individual flutter panel (see sketch)

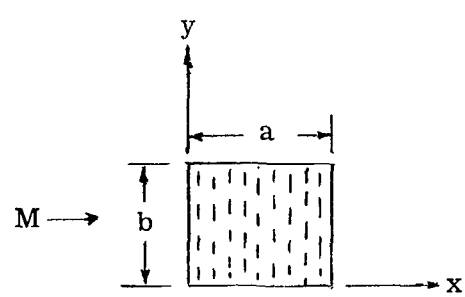

$$B = \mu \frac{a^4}{D_x} \omega^2 + n^2 \pi^2 \frac{a^2}{b^2} \frac{N_y a^2}{D_x} - n^4 \pi^4 \frac{a^4}{b^4} \frac{D_y}{D_x}$$

c,e,f quantities in stiffness expression (A4) (defined after eq. (A4))

D_c bending stiffness of corrugation-skin combination

D_d bending stiffness of "doubled plate" material between corrugations

D_e effective bending stiffness of total orthotropic plate

D_s plate bending stiffness of skin material, $\frac{Et_1^3}{12(1 - \nu^2)}$

D_x, D_y bending stiffnesses of orthotropic plate in x- and y-directions, respectively

$\overline{D}_x$ bending stiffness of a single corrugated section per unit width

D_{xy} twisting stiffness of orthotropic plate

d depth of corrugation sheet

E Young's modulus of corrugated panel material

$g = d - \overline{r}(1 - \cos \theta_o)$

$H = \frac{d}{r + \overline{r}} - 1$

h_1, h_2 quantities in stiffness expression (A6) (defined after eq. (A6))

$K = \frac{w - \overline{S} - S}{2(r + \overline{r})}$

$l = d - (r + \overline{r})(1 - \cos \theta_o)$

M Mach number

M_x bending moment applied normal to x-direction

M_1, M_2 bending moments applied to skin material and corrugation material, respectively

m	integer appearing in preflutter solution
N_x, N_y	applied in-plane forces for orthotropic plate (positive in compression) in x- and y-directions, respectively
n	integer appearing in exact flutter solutions
P	applied load in stiffness analysis
q	dynamic pressure
$r, \bar{r}$	radii of fillet curves on corrugation (see fig. 11)
$S, \bar{S}$	dimensions of corrugated panel (see fig. 11)
s_1, s_2, s_3	widths of equivalent corrugation (see fig. 13)
t_1, t_2	thicknesses of skin material and corrugation material, respectively
u_1, u_2, u_3	deflections of equivalent corrugation (see fig. 13)
W_n	deflection function
w	pitch of corrugation
x, y	Cartesian coordinates of orthotropic plate
α, δ, ϵ	parameters appearing in exact flutter solution
$\beta = \sqrt{M^2 - 1}$	
γ	length of portion of corrugation (see fig. 11)
Δp	pressure differential across panel (positive outward)
θ_o	slope of corrugation (see fig. 11)
λ	dynamic-pressure parameter, $\frac{2qa^3}{\beta D_x}$
λ_{ex}	experimental dynamic-pressure parameter

λ_p preflutter dynamic-pressure parameter

μ mass of orthotropic plate per unit area

ν Poisson's ratio (assumed to be 1/3 for numerical calculations)

ω circular frequency

PANELS, APPARATUS, AND TEST PROCEDURE

Panels

Flutter results for two types of flat rectangular panels are presented: corrugation-stiffened panels and unstiffened panels. These two types are discussed separately.

Corrugation-stiffened panels.- Two series of corrugation-stiffened panels were tested. The pertinent dimensions, materials, and stiffnesses (calculated by the method of appendix A) are given in table I. All these panels were tested with the airflow direction normal to the axis of the corrugations. The panels were assumed essentially to be simply supported in the flow direction (that is, at the leading and trailing edges).

The nine panels of the first series had the ends of each corrugation essentially free and are called free-edge panels herein. Details of these panels are shown in figure 1.

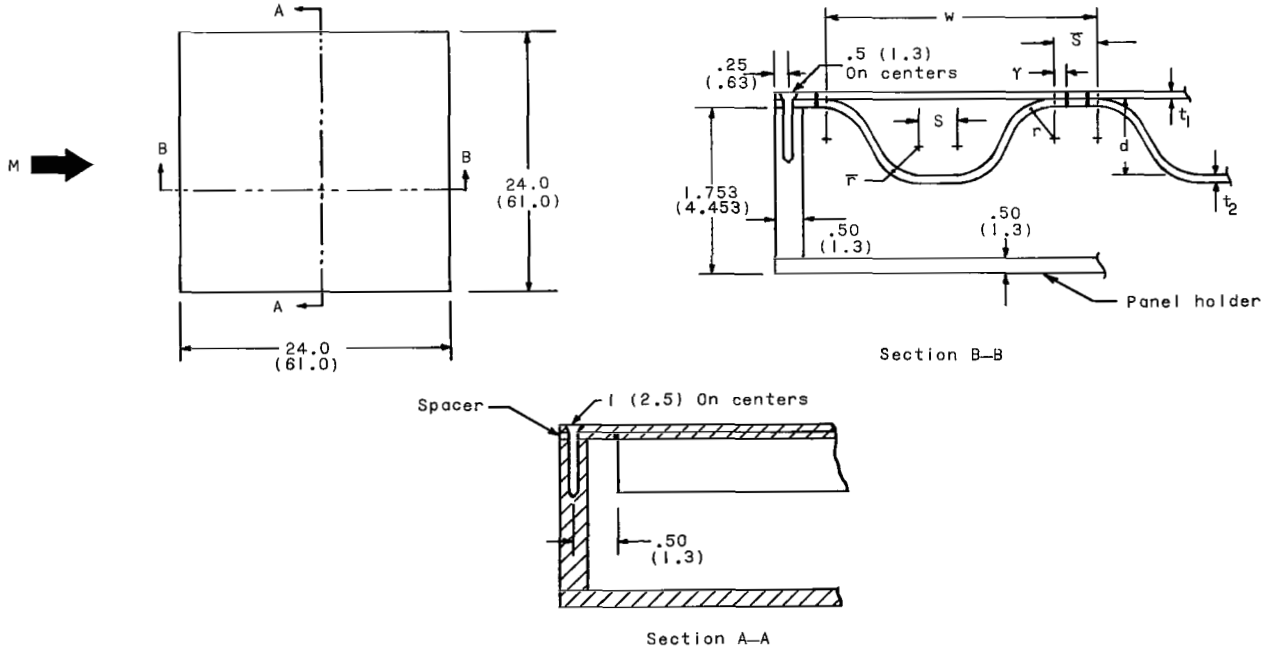

Figure 1.- Corrugation-stiffened panels with ends of corrugations free along longitudinal edges. All dimensions are given first in inches and parenthetically in centimeters.

The panels were 24.0 inches (61.0 cm) square, and had the corrugations ending approximately 0.25 inch (0.63 cm) from the supporting edge, with only the thin skin carried over the support (see section A-A). These panels are designated by the letter "U," "V," or "H" (hat), which describes the cross-sectional shape of a single corrugation.

Details of the ten panels of the second series, on which the corrugations were directly attached to the support fixture at their ends, are shown in figure 2. The attachment was accomplished by crushing the ends of the corrugations and allowing this thick crushed region to extend over the panel support. These panels are called crushed-edge panels herein, and were 37.3 inches (94.7 cm) long and 24.2 inches (61.5 cm) wide with S-shaped corrugations. (See fig. 2.) These crushed-edge panels are designated by the letter "S."

The panels designated S and V had a single weld line between the corrugations, whereas the panels designated U and H had double weld lines.

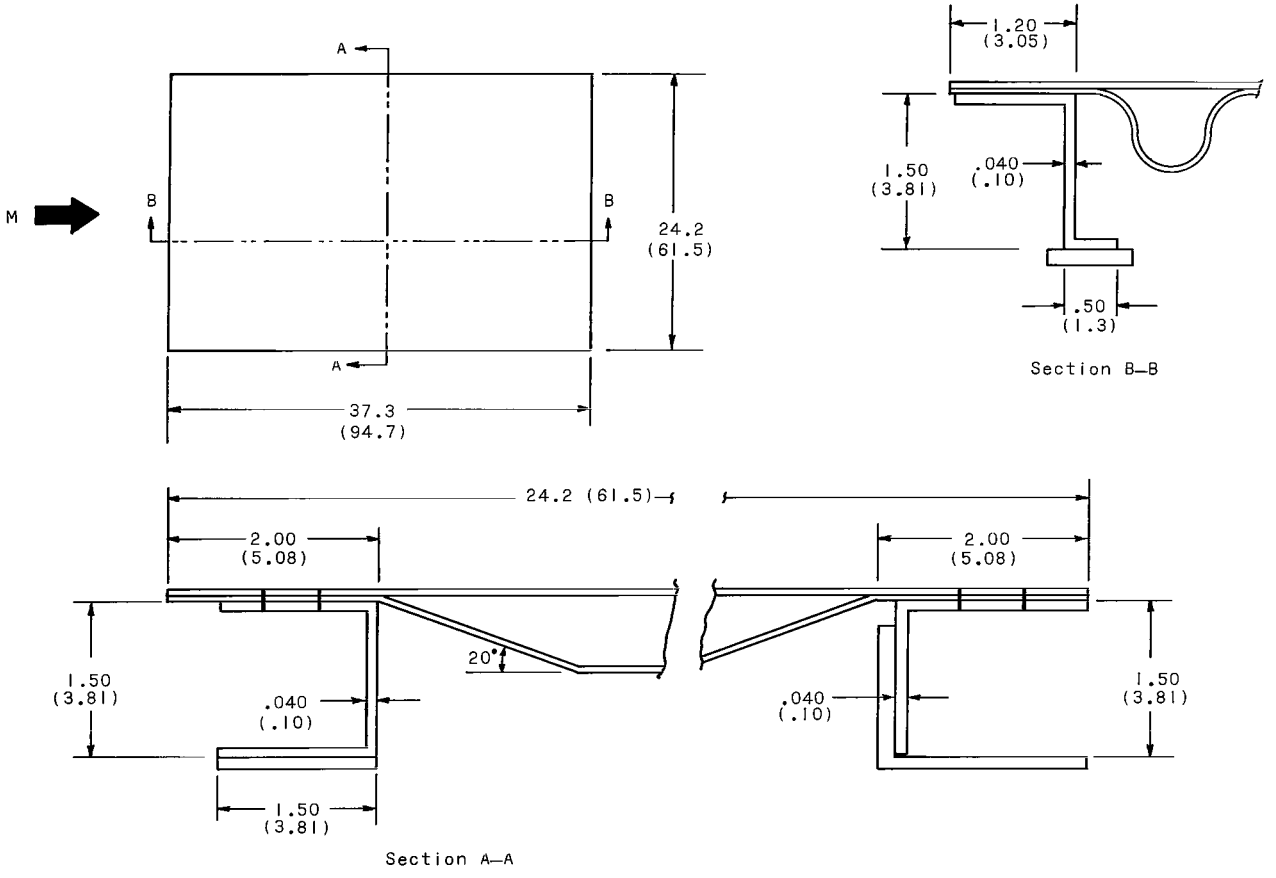

Figure 2.- Corrugation-stiffened panels with corrugations crushed along longitudinal edges. All dimensions are given first in inches and parenthetically in centimeters.

Unstiffened panels.- Two series of flat unstiffened rectangular panels were tested. The details of these panels are shown in figure 3, and the materials and dimensions are listed in table II. The four panels of the first series were divided into several bays in the cross-flow direction and were termed "multi-bay panels." The two-edge bays were equal in width but narrower than the remaining bays in order that the total width of each panel assembly remain 24.2 inches (61.5 cm). The length-width ratios of these multi-bay panels were approximately 6 and 10. The two panels of the second series were 24.2 inches (61.5 cm) wide and were termed "single-bay panels" (with length-width ratios a/b of 1 and 1.54).

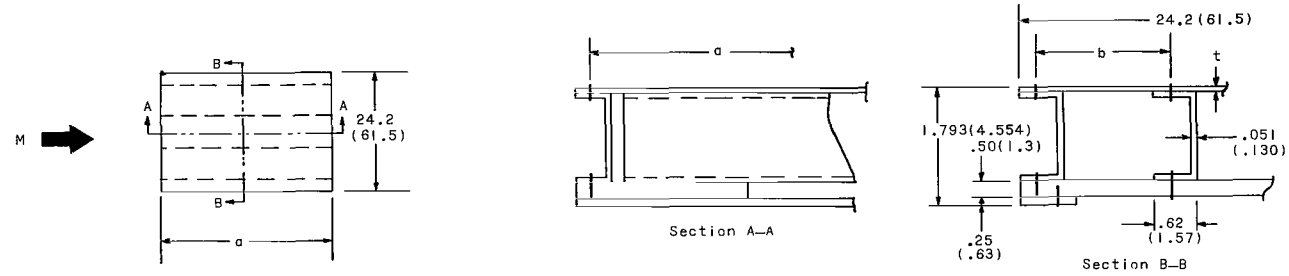

(a) Multi-bay panels.

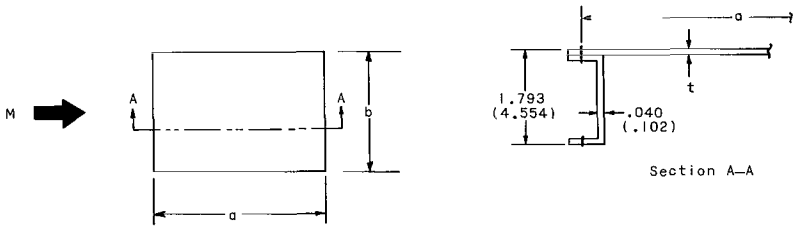

(b) Single-bay panels.

Figure 3.- Dimensions of flat unstiffened panels. All dimensions are given first in inches and parenthetically in centimeters.

Test Setup

The panel flutter tests discussed herein were conducted at the Langley Unitary Plan wind tunnel in the fixture shown in figures 4 and 5 and discussed in reference 12. This test fixture allows any panel up to approximately 3 feet (0.91 m) long by 2 feet (0.61 m) wide to be mounted, the reversible vertical splitter plate holding the panel 33 inches (0.84 m) from the glass observation wall. (See fig. 5.) The pressure distributions for this test fixture are shown in reference 13 and are noted there as being nonuniform, particularly at the low Mach numbers. Tests were run in the low Mach number test section of the Langley Unitary Plan wind tunnel where dynamic pressure can be varied

L-59-3993.1

Figure 4.- Test fixture with panel mounted in test section.

continuously from 130 to 2600 psf (6 to 124 kN/m^2) and Mach numbers from 1.57 to 2.87 are easily obtainable. The stagnation temperature of this tunnel can be varied slightly, but was held at 125° F (325° K) for most of the tests reported herein.

The pressure loading across the panels was also varied in these tests. The pressure differential is considered to be the difference in pressure between the cavity behind the panel and a static-pressure orifice located 9 inches (23 cm) ahead of the leading edge of the panel. A positive pressure differential indicates a higher pressure in the panel cavity. This pressure differential can be regulated or held constant (as the test requires) by means of a pump and servo arrangement; however, it is not completely uniform over the entire panel surface. (See ref. 13.) In all tests, six variable-reluctance-type deflectometers and an oscilloscope (with associated equipment) were used to monitor the motion of the panels. Both high-speed (16-mm) and low-speed (8-mm) motion pictures were taken to observe the motion of the panels at flutter.

Test Procedure

Since it is easier to vary the dynamic pressure than to change the Mach number in the tunnel, the following test procedure was adopted: For any given panel, a low Mach number was selected and either a low dynamic pressure or large differential pressure was established. Then, holding the dynamic pressure and Mach number constant, the pressure differential across the panel was varied in an attempt to initiate flutter. Flutter was defined as the combination of aerodynamic forces and pressure differential that caused the panel motion to become regular and its amplitude to exceed a predetermined arbitrary magnitude which was selected to exclude forced dynamic motion but not flutter (whether or not destruction of the panel occurred). If flutter did not occur, the dynamic pressure was increased by a preselected amount and the pressure differential was varied again. This procedure was continued until the flutter conditions were determined for the panel at that Mach number. Then the Mach number was increased a selected amount and the procedure was repeated again.

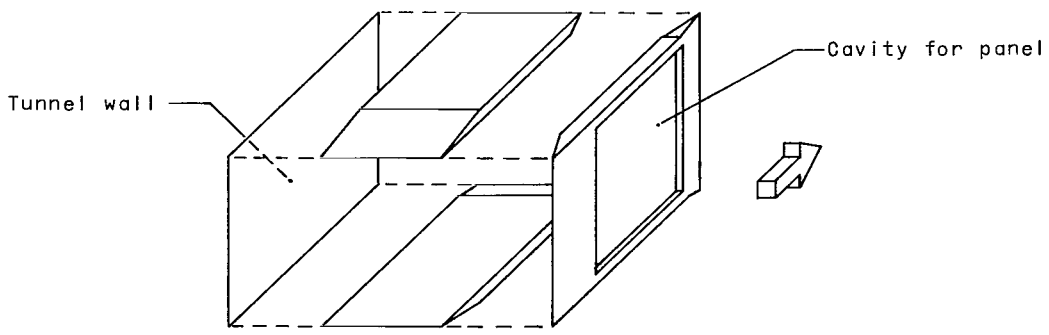

(a) Exploded view of splitter-plate arrangement.

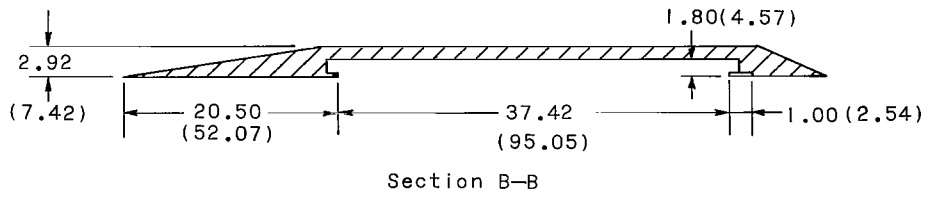

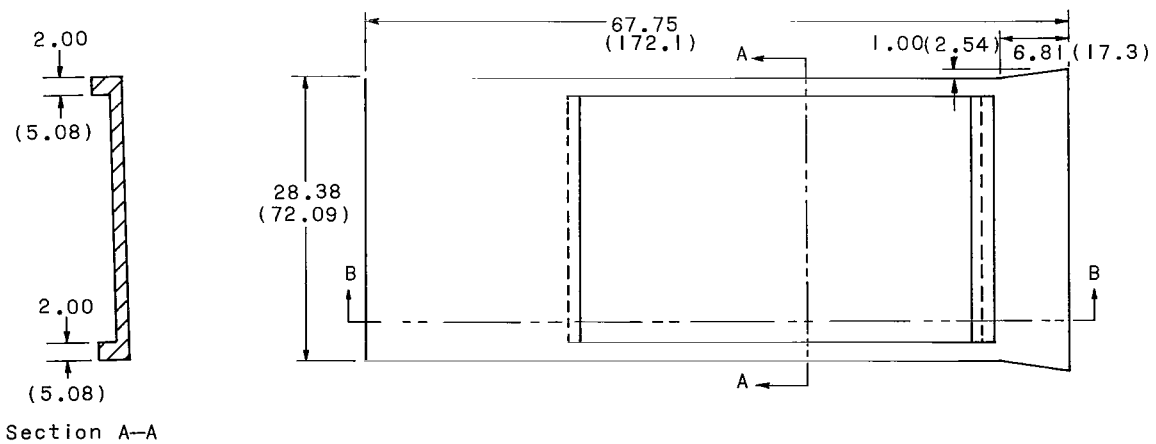

(b) Vertical splitter plate for mounting test panel.

Figure 5.- Test-panel holder. All dimensions are given first in inches and parenthetically in centimeters.

RESULTS AND DISCUSSION

Corrugation-Stiffened Panels

Typical results of tests of corrugation-stiffened panels are shown in figure 6, where the variation of dynamic pressure and pressure differential are shown for several cases. For a given panel and Mach number, the tests proceeded in the manner indicated by the arrows. Straight lines indicate no flutter conditions and serrate lines indicate flutter. The lowest dynamic pressure at which a given panel fluttered was defined as the critical dynamic pressure for that panel at that Mach number. The pressure differential across the panel at the initiation of flutter was used to define the actual critical flutter point as shown in figure 6. However, the pressure differential is only approximate since the flow conditions over the panel are not completely uniform. (See ref. 13.) Generally, from plots such as figure 6, it can be seen that an increase in pressure differential (either positive or negative) stopped the flutter motion of the panel.

In some cases, approximately the same magnitude of either positive or negative pressure differential was needed to stop flutter (see figs. 6(a) and 6(b)). In other cases, however, a somewhat erratic behavior occurred, as shown in figure 6(c), and, for these cases, large positive pressure differentials were generally required to initiate flutter.

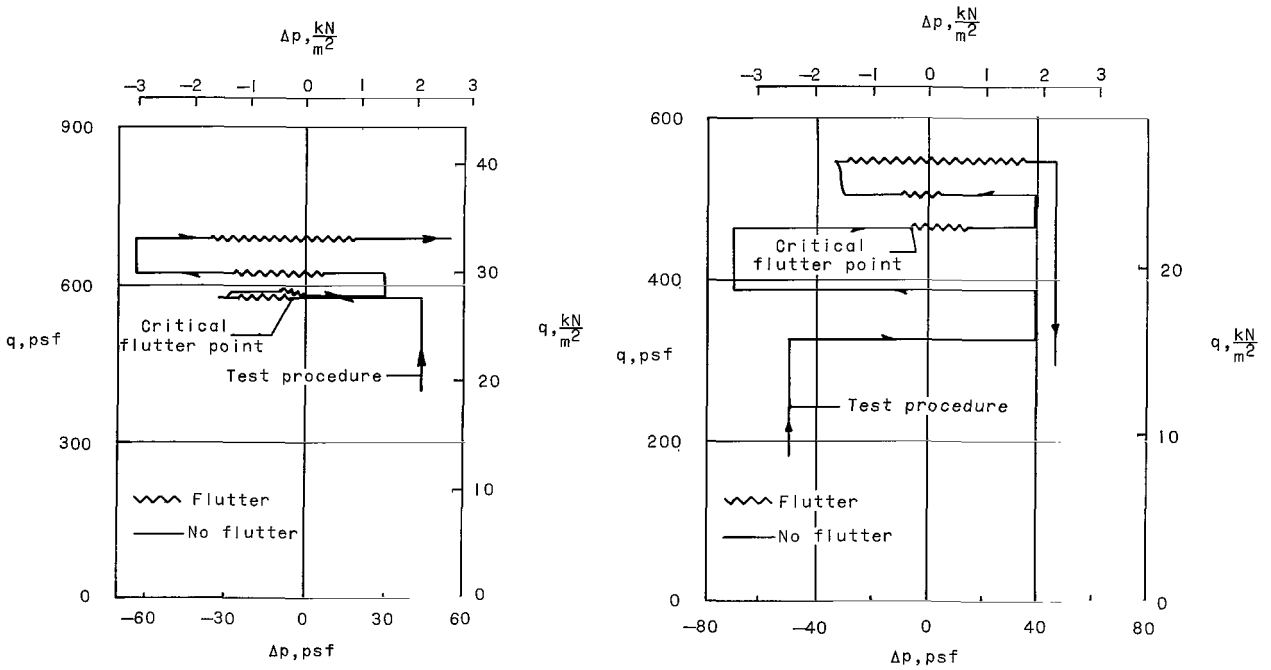

(a) Panel V-2; M = 1.96.

(b) Panel V-5; M = 1.84.

Figure 6.- Typical test data for corrugation-stiffened panels.

The reason for these results could be initial imperfections in the panels. However, this information cannot be determined from the data since no means for measuring such effects were provided.

The results of the flutter tests of corrugation-stiffened panels are presented in table III, where for each panel at specific Mach numbers the values of q and Δp for the "critical flutter point" are presented. These results are also shown plotted in figure 7 in terms of the critical dynamic-pressure flutter parameter $\lambda^{1/3}$ $\left(\text{where } \lambda = \frac{2qa^3}{\beta D_x}\right)$ and a parameter A/π^2. In the general case (for panels simply supported on all edges), A can be written as

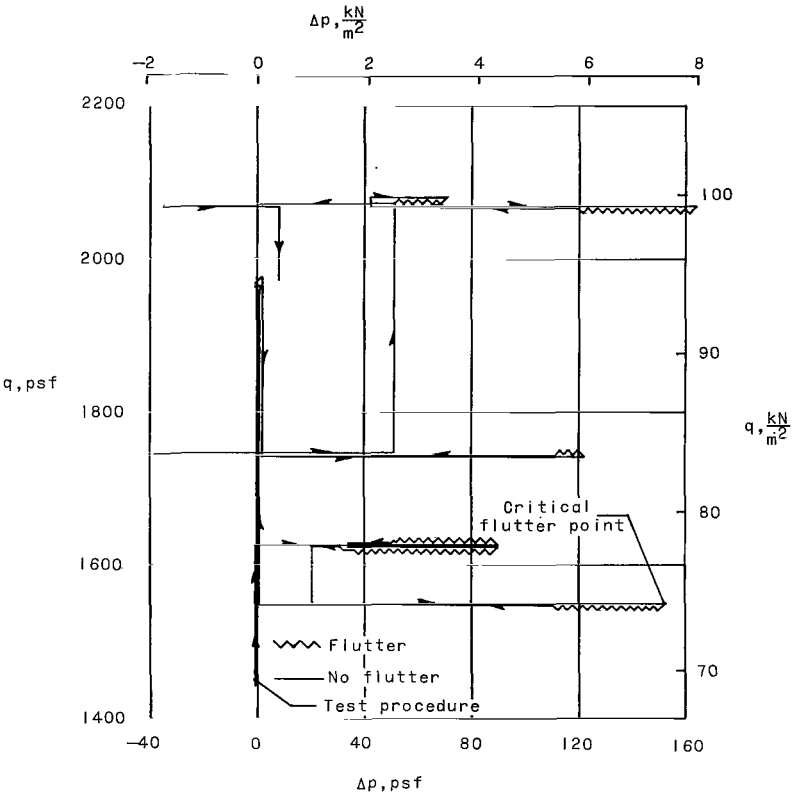

(c) Panel V-6; M = 1.84.

Figure 6.- Concluded.

$$A = \frac{N_x a^2}{D_x} - 2n^2\pi^2 \frac{a^2}{b^2} \frac{D_{xy}}{D_x} \tag{1}$$

which combines a length-width ratio term and an in-plane loading term. Herein, a and b refer to the length and width of the panel, respectively. N_x is the in-plane compressive load in the airflow direction, D_x is the bending stiffness in the airflow direction, and D_{xy} is the twisting stiffness of the panel. Since the in-plane forces could not be either directly varied or measured in this investigation, the in-plane forces were assumed to be zero and the first term in the expression for A (eq. (1)) was neglected when the test results were plotted. The quantity n is an integer associated with the number of half-waves in the cross-flow direction, and for all panels reported herein n was taken to be 1. The panel stiffnesses were computed by the method shown in appendix A and are presented in table I. The vertical I-shaped bars in figure 7 represent the

scatter of data measured for any given panel, and the designation by each bar or point refers to the corrugation shape and panel number given in table I.

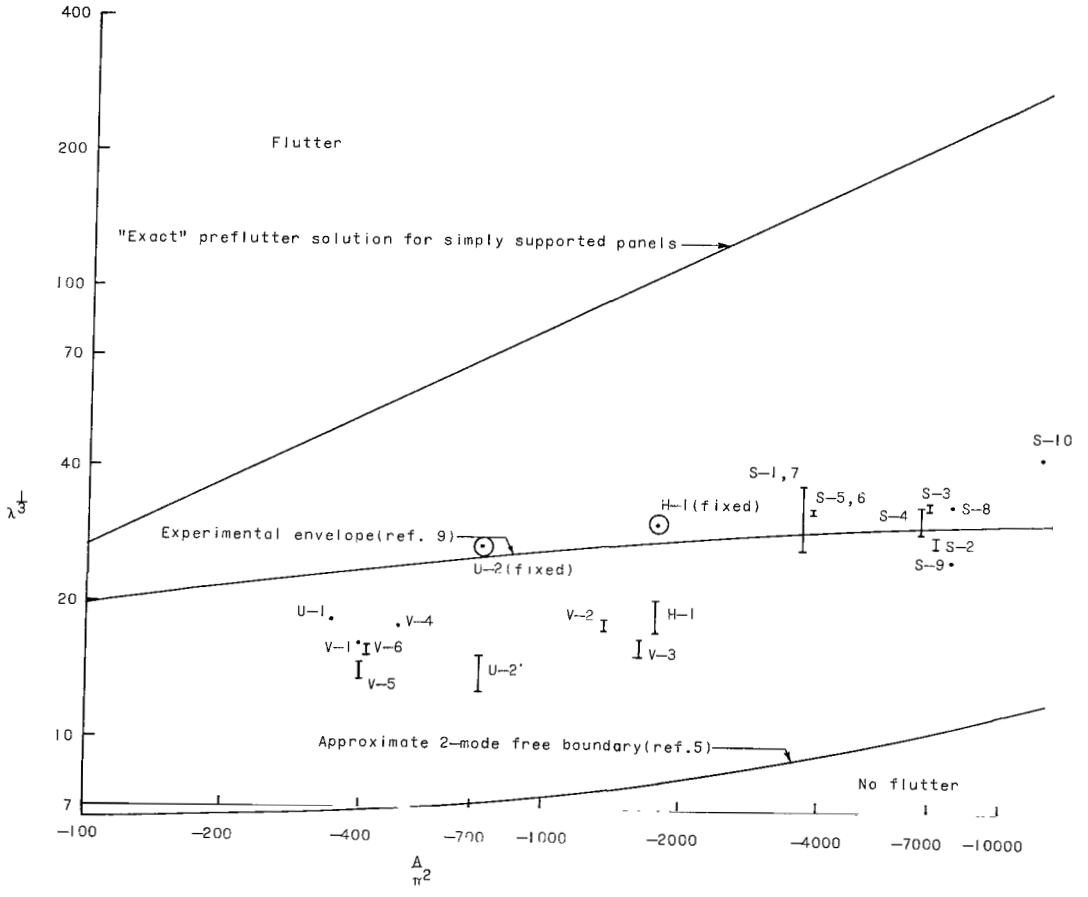

Figure 7.- Results of flutter tests on corrugation-stiffened panels.

The large scatter of flutter results for a single panel indicates that effects other than those incorporated in λ and A which are important in panel flutter were probably present during testing. One effect is the pressure differential mentioned previously. The influence of boundary conditions at the ends of the corrugations (cross-stream boundary conditions) are also seen to be important, since the crushed-edge panels (designated S) fluttered at significantly higher values of the dynamic-pressure parameter than the free-edge panels (designated U, V, and H). This fact is further verified by the test results from another investigation of corrugation-stiffened panels. (See ref. 8.) In reference 8, two of the free-edge panels were attached to the support fixture at the corrugation ends by angle clips. (See fig. 8.) The two panels selected for this adjustment were U-2 and H-1; some results of flutter tests on these panels are also shown in reference 8. The panel U-2 (fixed) should flutter (for zero thermal stress) at a dynamic pressure near

3400 psf (163 kN/m^2) and panel H-1 (fixed) should flutter at a dynamic pressure near 2900 psf (139 kN/m^2) both at a Mach number of 3.0. These two data points are shown in figure 7 as circled points. As can be seen from these two data points, attaching the ends of the corrugations to the support fixture caused significantly higher dynamic pressures for initiation of flutter than for identical free-edge panels. Therefore, the attachment of the ends of the corrugation greatly increases the flutter resistance of a corrugation-stiffened panel. (This result is also noted in ref. 8.)

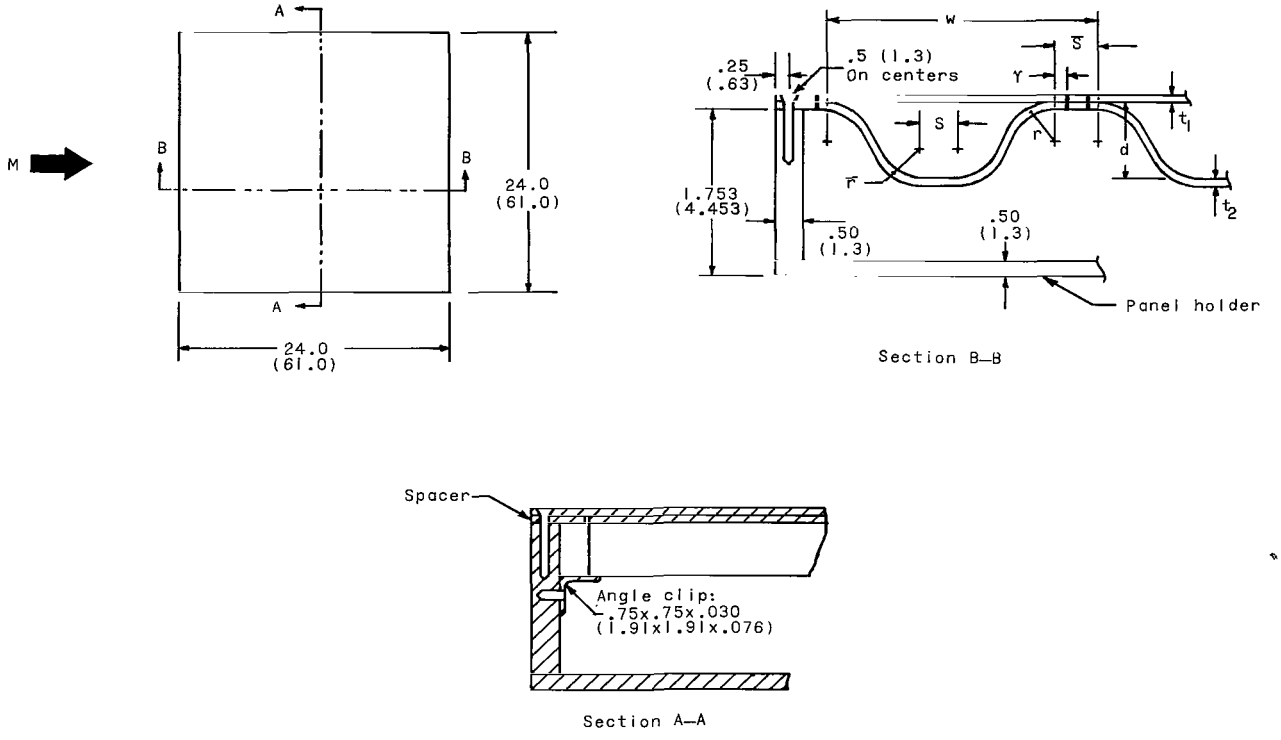

Figure 8.- Corrugation-stiffened free-edge panels modified to approximate clamped edges (from ref. 8).

This effect can be explained by assuming that the panels effectively end where the corrugations either end or are crushed. The remaining portion of the panel must be considered as a flexible support. With this assumption, the free-edge panels, the modified free-edge panels, and the crushed-edge panels could be idealized as shown in figure 9. The three boundary conditions investigated can be considered to be special cases of an orthotropic plate supported on a general elastic-edge support. The transverse flexibility of the panel support determines the deflectional spring constant for the general case, whereas the rotational flexibility of the panel support determines the torsional spring constant.

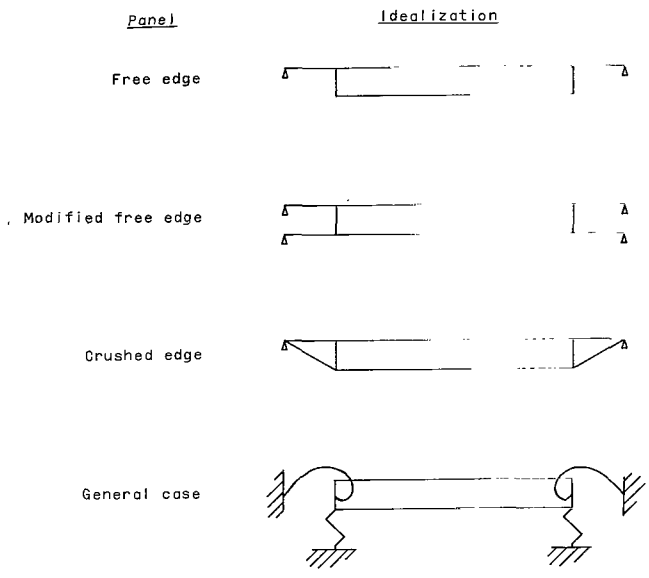

Figure 9.- Boundary-condition idealization.

From these idealizations, it can be seen that the free-edge panel supports correspond to the general case with a relatively small amount of transverse stiffness and negligible rotational stiffness. The modification of the free-edge panel supports (by addition of an angle clip) supplies a rotational stiffness and increases the transverse stiffness somewhat. The crushed-edge panel support supplies not only rotational stiffness but also an appreciable amount of transverse stiffness as well. Each stiffness increase causes an increase in the critical dynamic pressure for flutter. All these conclusions are borne out by the experimental results shown in figure 7. A similar conclusion was noted in reference 14, where improved agreement between theory and experiment was obtained with the use of an estimated value of this spring constant. The effect of these edge conditions is discussed in the next section.

The crushed-edge panels also fluttered at higher values of the dynamic-pressure parameter λ than the free-edge panels. The mode of failure for these two groups of panels was entirely different. The crushed-edge panels failed quickly and catastrophically, and the downstream ends of the panels were destroyed. The free-edge panels, on the other hand, fluttered for some time at several amplitude levels before small cracks formed in the skin at the ends of the corrugations. These panels still maintained their integrity even after cracks appeared. A similar dependency of mode of failure on the flexibility of edge supports were noted in reference 8.

Unstiffened Panels

The results of the flutter tests on flat unstiffened single-bay and multi-bay panels are presented in table IV. The panel numbers are the panel designations given in table II. For each Mach number used, the dynamic pressure and pressure differential on the panel at the flutter are listed for the conditions discussed under the column heading "Flutter Motion and Comments."

These test results are also shown plotted in figure 10 in terms of $\lambda^{1/3}$ and A/π^2. In plotting the data, the in-plane forces were assumed to be zero, as was done with the corrugation-stiffened panels. The vertical I-shaped bars in figure 10 again represent

scatter in the results, and indicates that other effects (pressure differential, for example) seem to be important for flat unstiffened panels.

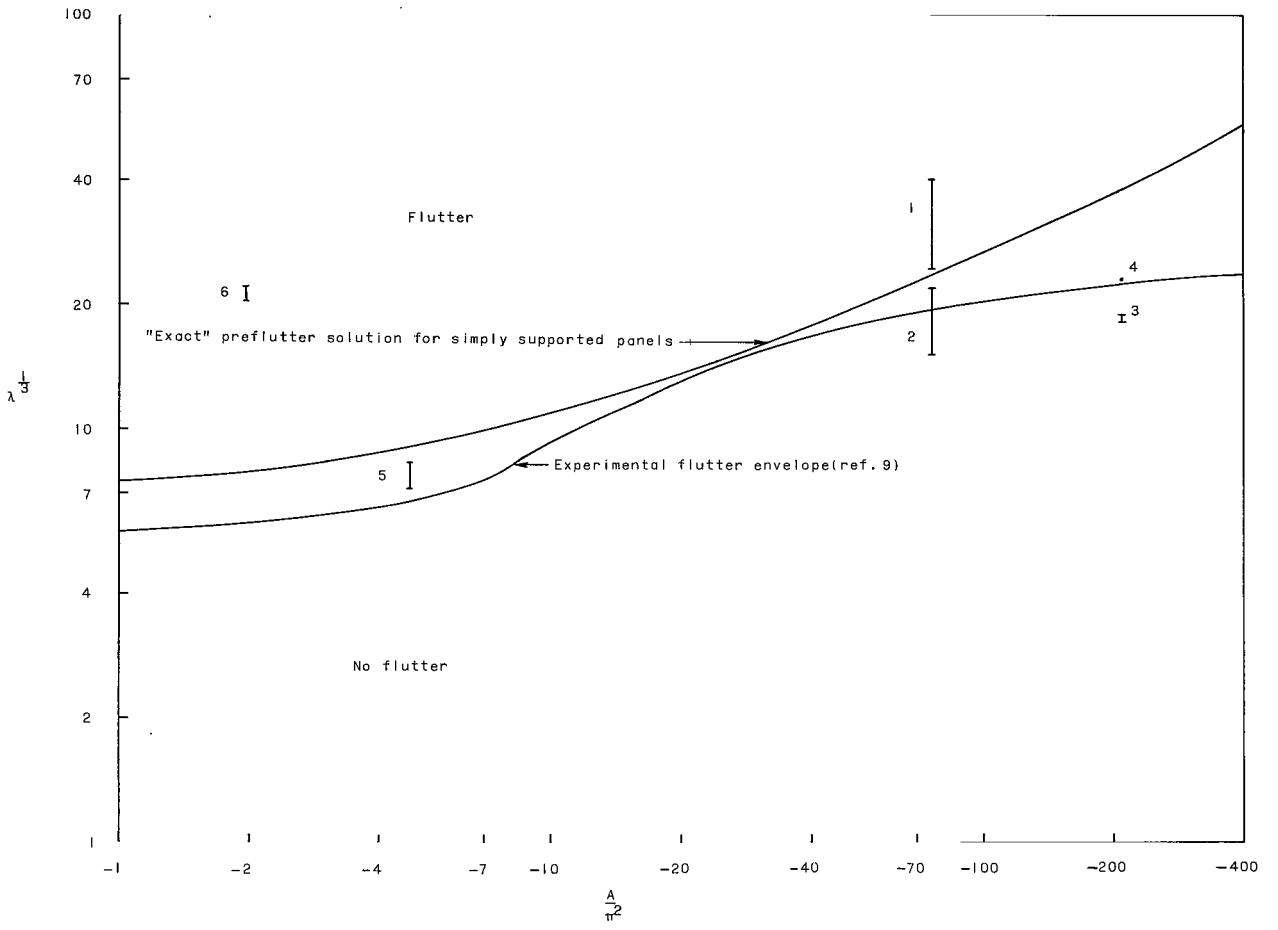

Figure 10.- Results of flutter tests on flat unstiffened panels.

COMPARISON OF TEST RESULTS WITH THEORY

As a simple means for comparing experimental results with theory, a preflutter solution can be written that is both easy to compute and accurate in the region of corrugation-stiffened panels. The "exact" solution from reference 2 assumes small deflections and thin-plate theory with static aerodynamic forces for a simply supported panel. The differential equation for the deflection W_n (eq. (5) of ref. 2) then becomes

$$W_n^{IV} + AW_n'' + \lambda W_n' - BW_n = 0 \qquad (2)$$

When this equation is solved exactly, it yields the eigenvalue equation (eq. (9) of ref. 2)

$$\left(\epsilon^2 + \delta^2\right)^2 + 4\alpha^2\left(\delta^2 - \epsilon^2\right)\sin\,\delta\,\sinh\,\epsilon = 8\alpha^2\epsilon\,\delta\left(\cosh\,\epsilon\,\cos\,\delta - \cosh\,2\alpha\right) \tag{3}$$

where

$$\left.\begin{aligned} \delta &= \sqrt{\frac{\lambda}{4\alpha} + \alpha^2 + \frac{A}{2}} \\ \epsilon &= \sqrt{\frac{\lambda}{4\alpha} - \alpha^2 - \frac{A}{2}} \\ B &= \frac{\lambda^2}{16\alpha^2} - 4\left(\alpha^2 + \frac{A}{4}\right)^2 \end{aligned}\right\} \tag{4}$$

and α is a parameter that is varied until equation (3) is satisfied for any given values of A and λ. The definition of the quantities in equation (2) for orthotropic plates (from ref. 9) are given in the notation of the present paper as

$$\left.\begin{aligned} A &= \frac{N_x a^2}{D_x} - 2n^2\pi^2\,\frac{a^2}{b^2}\,\frac{D_{xy}}{D_x} \\ B &= \mu\,\frac{a^4}{D_x}\,\omega^2 + n^2\pi^2\,\frac{a^2}{b^2}\,\frac{N_y a^2}{D_x} - n^4\pi^4\,\frac{a^4}{b^4}\,\frac{D_y}{D_x} \\ \lambda &= \frac{2qa^3}{\beta D_x} \end{aligned}\right\} \tag{5}$$

By following the method of Movchan (ref. 15), a solution of the "exact" eigenvalue equation (eq. (3)) which yields conservative estimates of the flutter boundary can be shown to exist. Equation (3) is thus seen to be satisfied if $\delta = \pm 2m\pi$ and $\epsilon = 2\alpha$. Substituting these values into equations (4) yields the preflutter solution for the critical flutter parameter as

$$\lambda_p = 8\left(m^2\pi^2 + \frac{4m^2\pi^2 - A}{6}\right)\sqrt{\frac{4m^2\pi^2 - A}{6}} \tag{6}$$

For panels with the axis of the corrugations normal to the direction of flow, the twisting stiffness D_{xy} is much larger than the bending stiffness D_x, and, thus, for small

compressive forces N_x, negative values of A result. (See eqs. (5).) In this case, λ_p has a minimum value when $m = 1$ (this value of m corresponds to the coalescence of the first two mode shapes only and may be somewhat in error). When $m = 1$, equation (6) becomes

$$\lambda_p = 16.878\left(10 - \frac{A}{\pi^2}\right)\sqrt{4 - \frac{A}{\pi^2}} \tag{7}$$

This preflutter solution is compared in the following table with the exact solution of the eigenvalue equation (eq. (3)):

$\frac{A}{\pi^2}$	λ_p	λ_{ex}
-0	337.56	341
-10	1 263.0	1 314
-20	2 480.6	2 602
-100	18 932	19 390
-1 000	540 120	542 220
-10 000	16 898 000	16 904 000

From this comparison, it can be seen that the preflutter solution does agree very closely with the "exact" solution for large negative values of A for simply supported panels. This preflutter solution may now be compared with the experimental results to determine the actual applicability of such an approach.

Corrugation-Stiffened Panels

The experimental flutter results for the corrugation-stiffened panels presented in table III are compared with the exact preflutter solution in figure 7. From the figure it is seen that the agreement between the experimental results and the exact preflutter solution for simply supported panels is extremely poor, the agreement becoming even worse for large negative values of A. Since it appears from the test results that boundary conditions in the cross-flow direction can be important, an additional theoretical curve (from ref. 5) has been added to figure 7. This curve is the result of an approximate two-mode Galerkin solution for free-edge panels with stiffnesses roughly equal to those of the corrugation-stiffened panels tested. The experimental data are seen to be between the curve for the preflutter solution for the simply supported panels and the curve for the Galerkin solution of the free-edge panels. This fact suggests that the test panels were

somewhere between completely free and simply supported with respect to deflection of the corrugation ends.

The experimental flutter envelope from reference 9 is shown in figure 7; this curve also falls between the two theoretical curves. Even though use of the flutter envelope of reference 9 as a design criterion could result in unnecessary weight penalties in some cases with a possibility of being unconservative on occasion, this type of curve appears to be the best available means for the prediction of the flutter boundary for corrugation-stiffened panels at present. It may be noted from figure 7 that the crushed-edge panels generally flutter as a group at values of $\lambda^{1/3}$ above those of the flutter envelope, whereas all the free-edge panels fluttered at values of $\lambda^{1/3}$ below the flutter envelope. This result indicates that the experimental envelope is a reasonable curve for elastically supported panels. It should also be pointed out that some of the difference between the curve for simply supported panels and the experimental results could also be due to the fact that the actual transverse shear stiffnesses of these panels are not infinite as is assumed in the theoretical calculations. The influence of these shearing stiffnesses could be appreciable and this problem is discussed in reference 5.

Unstiffened Panels

The experimental flutter results for the flat unstiffened panels presented in table IV are compared in figure 10 with the preflutter solution presented previously. This preflutter solution is only in fair agreement with the experimental flutter results and is unconservative for larger negative values of A/π^2. The experimental envelope from reference 9 is also shown plotted in figure 10, and agreement between this theoretical curve and the experimental data is fairly good, particularly at larger values of A/π^2. This curve is only slightly unconservative in this region and can be considered adequate throughout the entire region shown.

CONCLUSIONS

Upon investigation of the experimental results obtained from tests of 19 corrugation-stiffened panels and 6 flat unstiffened panels, several important facts appear evident:

1. A flutter envelope drawn to encompass all experimental results available at any given time seems to be, at present, the best means for predicting the flutter boundary for corrugation-stiffened panels. Theoretical methods currently available are not adequate to predict the flutter characteristics of a general panel. The flutter envelope from NASA TN D-451 agrees with the test results for isotropic panels fairly well. The agreement for crushed-edge orthotropic panels is fair, but the agreement for free-edge orthotropic panels is poor. The reason for this poor agreement is that panels with free edges were not used to define the flutter envelope.

2. The mode of failure for panels with free-edge corrugations is vastly different than the mode of failure for the crushed-edge panels. The free-edge panels started to flutter at much lower dynamic pressures and continued to flutter for a considerable length of time before cracks appeared in the skin; even then panel integrity was maintained. The crushed-edge panels, however, withstood a much higher dynamic pressure before flutter, but when flutter occurred it was quick and catastrophic.

3. The flutter results are not functions only of the flutter parameter and the in-plane loading factor but are also greatly affected by several other effects that are not incorporated in these parameters. Several of the effects that should be included are

(a) The influence of pressure differential across the panel.

(b) The influence of boundary conditions in the cross-flow direction. The experimental results show that changing the boundary conditions in the cross-flow direction can change the flutter dynamic pressure by a large factor, and the influence of these boundary conditions must be investigated.

(c) The influence of using a finite shear stiffness for any given panel. The corrugation-stiffened panels are far from infinitely stiff when resisting a shearing load, and thus the influence of this shear stiffness might be of importance for this type of flutter panel.

Langley Research Center,
National Aeronautics and Space Administration,
Langley Station, Hampton, Va., October 6, 1965.

APPENDIX A

STIFFNESSES OF FLAT PANELS REINFORCED BY A CORRUGATED SHEET

Since it is a common practice in the aircraft industry to construct skin panels of a corrugation-sheet combination, the flutter characteristics of such panels must be investigated. These panels may be considered as anisotropic plates and panel flutter theory may be applied; however, the stiffnesses of the panels must be determined first. The method of approach used herein is essentially the same as the method presented in reference 16. Several differences are noted where they occur, and all expressions are written in an easily usable form.

A schematic drawing of a single cell of a general panel composed of a skin sheet and a single corrugated-stiffener sheet is shown in figure 11. This general shape can be specialized to a square (hat) corrugation, a V-corrugation, or a U-corrugation by proper choice of the parameters. The heavy vertical marks between skin and corrugation indicate either weld or rivet junctions joining the two parts.

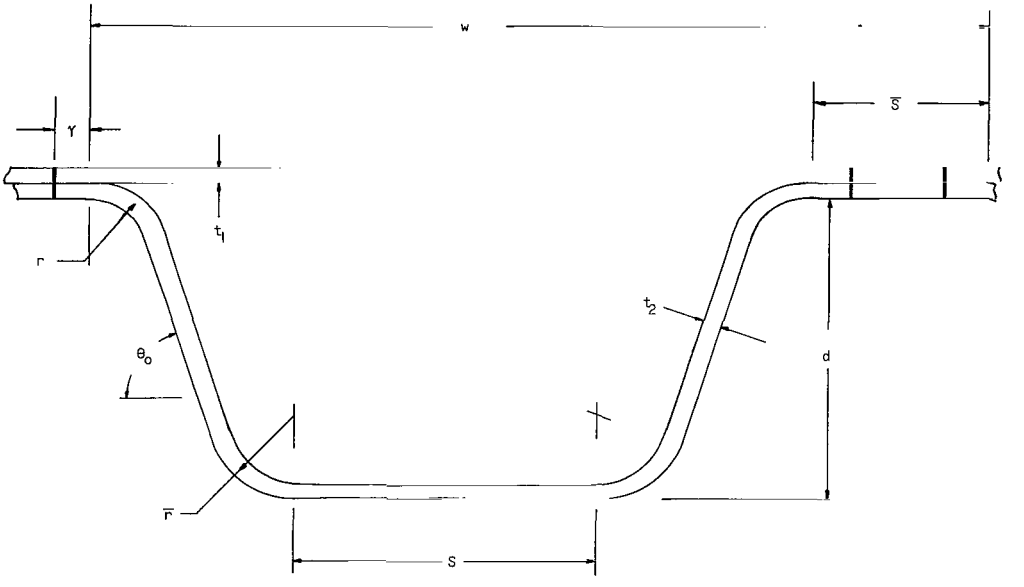

Figure 11.- Schematic drawing of general skin corrugation.

Bending Stiffness D_x

One approach to the problem of computing the bending stiffness D_x is to separate the skin sheet and the corrugation sheet and analyze each one individually, and then equate

their slopes and deflections at the weld line so that they can be joined again. The skin and corrugation are subjected to the loads and moments shown in figure 12. The load P is applied so that the horizontal displacement of the end of the corrugation (caused by the applied moment M_2) may be equated to the horizontal displacement of the cover sheet. By applying Castigliano's theorem as in reference 17 and by writing the strain energy of bending for both the corrugation sheet and the cover sheet, the displacements and slopes of both sheets can be determined at the weld line. Equating these expressions yields two equations involving P, M_1, and M_2, and these equations can be used to solve for the ratio of M_1 to M_2. The final equation needed is found by assuming that the stiffness of a panel is proportional to the moment it will carry, or

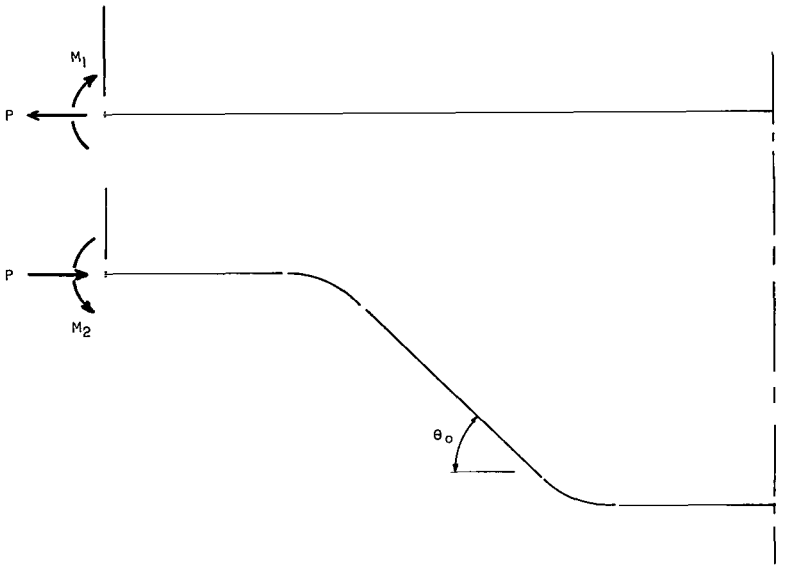

Figure 12.- Loads and moments used in analysis of stiffnesses of a general corrugation.

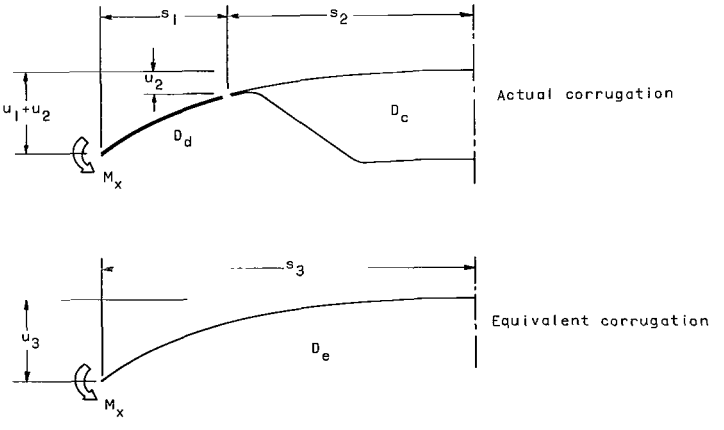

Figure 13.- Idealization of corrugation to an equivalent corrugation.

$$\frac{\bar{D}_x}{D_s} = \frac{M_1 + M_2}{M_1} = 1 + \frac{M_2}{M_1} \qquad \text{(A1)}$$

where $\bar{D}_x/D_s$ is the ratio of the stiffness of the combination of the skin and corrugation to the stiffness of the skin alone. Thus the stiffness is determined for the bent portion of the corrugation between welds. The stiffness of the short section of "doubled" plate between the welds of adjacent corrugations must also be taken into account.

There are several ways of doing so. The method selected herein replaces the two sections of corrugated panel by a single panel section with an equivalent stiffness so that the deflection of the actual panel and the equivalent panel are the same under a moment applied at the tip, as shown in figure 13. Thus,

APPENDIX A

$$\left.\begin{aligned} u_1 + u_2 &= \frac{M_x}{2D_c}\left(s_2^2 + 2s_1s_2 + s_1^2\frac{D_c}{D_d}\right) \\ u_3 &= \frac{M_x s_3^2}{2D_e} = u_1 + u_2 \end{aligned}\right\} \tag{A2}$$

Now the equivalent stiffness D_e can be computed if the component stiffnesses are known. The stiffness of the bent corrugation D_c has been calculated from equation (A2) as $\overline{D}_x$. The stiffness of the doubled sheet D_d is assumed to be the stiffness of a plate of thickness $t_1 + t_2$. Thus, from equation (A2), the equivalent stiffness ratio D_x/D_s in the x-direction is

$$\frac{D_x}{D_s} = \frac{\overline{D}_x/D_s}{1 + \left(\frac{\overline{S} - 2\gamma}{w}\right)^2\left[\frac{\overline{D}_x}{D_s}\left(\frac{t_1}{t_1 + t_2}\right)^3 - 1\right]} \tag{A3}$$

where the stiffness of the corrugation cell per unit width $\overline{D}_x/D_s$ is

$$\frac{\overline{D}_x}{D_s} = 1 + \left(\frac{t_2}{t_1}\right)^3 \frac{w - \overline{S} + 2\gamma}{2d}\frac{f}{fe - c^2} \tag{A4}$$

where

$$c = \left(\frac{r}{d}\right)^2(\theta_o - \sin\theta_o) + \left(\frac{\overline{r}}{d}\right)^2(\sin\theta_o - \theta_o\cos\theta_o) + \left(\frac{\overline{r}}{d}\right)\left(\frac{g}{d}\right)\theta_o + \frac{l^2}{2d^2\sin\theta_o} + \frac{r}{d}\frac{l}{d}\tan\frac{\theta_o}{2} + \frac{S}{2d}$$

$$e = \frac{\gamma}{d} + \left(\frac{r}{d} + \frac{\overline{r}}{d}\right)\theta_o + \frac{S}{2d} + \frac{l}{d\sin\theta_o}$$

$$f = \left(\frac{r}{d}\right)^3\left(\frac{3\theta_o}{2} - 2\sin\theta_o + \frac{\sin 2\theta_o}{4}\right) + \left(\frac{r}{d}\right)^2\left(\frac{l}{d}\right)\sin\theta_o\tan^2\frac{\theta_o}{2} + \left(\frac{r}{d}\right)\left(\frac{l}{d}\right)^2\tan\frac{\theta_o}{2} + \frac{S}{2d}$$

$$+ \left(\frac{l}{d}\right)^3\frac{1}{3\sin\theta_o} + \frac{\overline{r}}{d}\theta_o\left(\frac{g}{d}\right)^2 + 2\left(\frac{\overline{r}}{d}\right)^2\frac{g}{d}(\sin\theta_o - \theta_o\cos\theta_o) + \left(\frac{\overline{r}}{d}\right)^3\left(\frac{3\theta_o}{2} - \theta_o\sin^2\theta_o\right.$$

$$\left. - \frac{3}{4}\sin 2\theta_o\right)$$

with $\frac{l}{d} = 1 - \left(\frac{r}{d} + \frac{\overline{r}}{d}\right)(1 - \cos\theta_o)$ and $\frac{g}{d} = 1 - \frac{\overline{r}}{d}(1 - \cos\theta_o)$.

It may be noted that either θ_o of $\bar{S}$ need be given but not both. They are related by the following expression:

$$\bar{S} = w - S - 2 \sin \theta_o (r + \bar{r}) - 2l \cot \theta_o$$

or

$$\theta_o = \cos^{-1}\left(\frac{-H + K\sqrt{H^2 + K^2 - 1}}{H^2 + K^2}\right) \tag{A5}$$

where $H = \dfrac{d}{r + \bar{r}} - 1$ and $K = \dfrac{w - \bar{S} - S}{2(r + \bar{r})}$.

For panels with a single weld line between corrugations ($\gamma = \bar{S}/2$), the equivalent panel stiffness is given by equation (A4). This expression is equivalent to the corresponding expression (B19) from reference 16. For panels with a double weld line between corrugations, equation (A3) must be used, and this expression differs slightly from the corresponding expression (B33) of reference 16, where an equal change in slope between the two ends of the equivalent section was used as a criterion instead of equal deflection of the tip of the equivalent section as was used herein.

Bending Stiffness D_y

The bending stiffness of these panels in the direction of the corrugations D_y can be determined by calculating the moment of inertia per unit width of a panel with the cross section given in figure 11. However, it has been shown (ref. 4) that the stiffness of a panel perpendicular to the airflow (characterized by the parameter B) has little direct effect on the problem of panel flutter. All the corrugation-stiffened panels tested herein had their corrugations perpendicular to the airflow, and, therefore, the stiffnesses of these corrugated panels were not computed in the direction of the corrugations. If, however, the corrugations were alined with the airflow, the stiffness D_y would be important and must be computed. Therefore, this stiffness expression from reference 16 is included herein for completeness and is as follows:

APPENDIX A

$$\frac{D_y}{(1-\nu^2)D_s} = 1 + 12\left(\frac{h_1}{t_1} + \frac{1}{2} + \frac{t_2}{2t_1}\right)^2 + 12\,\frac{t_2}{t_1}\left(\frac{d}{w}\right)\frac{d^2}{t_1^2}\left\{\frac{h_1^2}{d^2}\,\frac{S}{d} + \frac{h_2^2}{d^2}\,\frac{\bar{S}}{d} + 2\theta_o\left(\frac{h_1^2}{d^2}\,\frac{r}{d} + \frac{h_2^2}{d^2}\,\frac{\bar{r}}{d}\right)\right.$$

$$+ \frac{l^3}{6d^3\sin\theta_o} + \left(4\sin\theta_o - 3\theta_o - \frac{\sin 2\theta_o}{2}\right)\left[\frac{r^2}{d^2}\left(\frac{h_1}{d} - \frac{r}{d}\right) + \frac{\bar{r}^2}{d^2}\left(\frac{h_2}{d} - \frac{\bar{r}}{d}\right)\right]$$

$$+ \left(\frac{\sin 2\theta_o}{2} - \theta_o\right)\left(\frac{r^2}{d^2}\,\frac{h_1}{d} + \frac{\bar{r}^2}{d^2}\,\frac{h_2}{d}\right) + \frac{2l}{d\sin\theta_o}\left(\frac{g}{d} - \frac{l}{2d} - \frac{h_1}{d}\right)^2 + \frac{t_2^2}{12d^2}\left[\frac{2l}{d}\left(\frac{1+\sin^2\theta_o}{\sin\theta_o}\right)\right.$$

$$\left.\left. + \left(\frac{r}{d} + \frac{\bar{r}}{d}\right)\left(3\theta_o - \frac{\sin 2\theta_o}{2}\right) + \frac{S}{d} + \frac{\bar{S}}{d}\right]\right\} \tag{A6}$$

where

$$\frac{h_1}{d} = \frac{-\frac{w}{d}\left(\frac{t_1+t_2}{2d}\right) + 2\,\frac{t_2}{t_1}\left[\left(\frac{r^2}{d^2} - \frac{\bar{r}^2}{d^2}\right)(\theta_o - \sin\theta_o) + \frac{l}{2d}\left(\frac{r}{d} - \frac{\bar{r}}{d}\right)\tan\frac{\theta_o}{2} + \frac{S}{2d} + \frac{\bar{r}}{d}\,\theta_o + \frac{l}{2d\sin\theta_o}\right]}{\frac{w}{d} + 2\,\frac{t_2}{t_1}\left(\frac{\bar{S}}{2d} - \frac{\gamma}{d} + e\right)}$$

and

$$\frac{h_2}{d} = 1 - \frac{h_1}{d}$$

Several small terms involving t_2^3 were added to the expression from reference 16 in order that equation (A6) could be consistent and include all terms involving t_2^3.

Twisting Stiffness D_{xy}

The twisting stiffness of corrugation-stiffened panels can be computed by considering the torsion-twist relationship for each corrugation cell. Thus, in reference 16, it is shown

$$\frac{D_{xy}}{D_s} = \frac{12A_o^2(1-\nu)}{\left(\frac{t_1^2}{d^2}\right)\frac{w}{d}\left(\frac{w}{d} - \frac{\bar{S}}{d} + \frac{2\gamma}{d} + 2\,\frac{t_1}{t_2}\,e\right)} \tag{A7}$$

where A_o is $1/d^2$ times the average area enclosed by the inside and outside of a corrugation cell. This nondimensional area can be written as

$$A_o = \left(\frac{t_1}{d} + \frac{t_2}{d}\right)\left(\frac{w}{d} - \frac{\bar{S}}{d} + \frac{2\gamma}{d}\right) + 2\left(\tan\frac{\theta_o}{2} - \frac{\theta_o}{2}\right)\left(\frac{r^2}{d^2} - \frac{\bar{r}^2}{d^2}\right) + \left(\frac{S}{d} + \cot\theta_o + 2\frac{\bar{r}}{d}\tan\frac{\theta_o}{2}\right) \quad \text{(A8)}$$

The twisting stiffness expression (eq. (A7)) differs from the corresponding expression in reference 9 (eq. (11)) by a factor of 2; the present result is smaller. This difference, however, is insignificant when computing flutter values for corrugation-stiffened panels since the flutter boundary curve of reference 9 is very flat in this region. This fact has been noted before. (See ref. 10.)

APPENDIX B

CONVERSION OF U.S. CUSTOMARY UNITS TO SI UNITS

The International System of Units (SI) was adapted by the Eleventh General Conference on Weights and Measures, Paris, October 1960, in Resolution No. 12 (ref. 11). Conversion factors for the units used herein are given in the following table:

Physical quantity	U.S. Customary Units	Conversion factor (*)	SI Units
Length	in.	0.0254	meters (m)
Moment	in-lbf	0.113	meter-newton (m-N)
Pressure	lbf/ft^2	47.88	newtons/$meter^2$ (N/m^2)
Temperature . .	($^oF + 459.67$)	5/9	degrees Kelvin (^oK)

*Multiply value given in U.S. Customary Unit by conversion factor to obtain equivalent value in SI unit.

Prefixes to indicate multiple of units are as follows:

Prefix	Multiple
kilo (k)	10^3
centi (c)	10^{-2}

REFERENCES

1. Eisley, J. G.: The Flutter of Simply Supported Rectangular Plates in a Supersonic Flow. OSR-TN-55-236, GALCIT, July 1955.

2. Hedgepeth, John M.: Flutter of Rectangular Simply Supported Panels at High Supersonic Speeds. J. Aeron. Sci., vol. 24, no. 8, Aug. 1957, pp. 563-573, 586.

3. Luke, Yudell L.; and St. John, Andrew: Supersonic Panel Flutter. WADC TR 57-252, U.S. Air Force, July 1957.

4. Bohon, Herman L.: Flutter of Flat Rectangular Orthotropic Panels With Biaxial Loading and Arbitrary Flow Direction. NASA TN D-1949, 1963.

5. Weidman, Deene J.: Effects of Side-Edge Boundary Conditions and Transverse Shear Stiffnesses on the Flutter of Orthotropic Panels in Supersonic Flow. NASA TN D-3302, 1966.

6. Cunningham, H. J.: Flutter Analysis of Flat Rectangular Panels Based on Three-Dimensional Supersonic Potential Flow. AIAA J., vol. 1, no. 8, Aug. 1963, pp. 1795-1801.

7. Dowell, E. H.; and Voss, H. M.: Experimental and Theoretical Panel Flutter Studies in the Mach Number Range 1.0 to 5.0. Paper No. 64-491, Am. Inst. Aeron. Astronaut., July 2, 1964.

8. Bohon, Herman L.: Experimental Flutter Results for Corrugation-Stiffened Panels at a Mach Number of 3. NASA TN D-2293, 1964.

9. Kordes, Eldon E.; Tuovila, Weimer J.; and Guy, Lawrence D.: Flutter Research on Skin Panels. NASA TN D-451, 1960.

10. Fung, Y. C.: On Corrugation-Stiffened Panels. SM 62-33(AFOSR 3122), Graduate Aeron. Labs., California Inst. Technol., June 1962.

11. Mechtly, E. A.: The International System of Units – Physical Constants and Conversion Factors. NASA SP-7012, 1964.

12. Trussell, Donald H.; and Weidman, Deene J.: A Radiant Heater to Simulate Aerodynamic Heating in a Wind Tunnel. NASA TN D-530, 1960.

13. Tuovila, Weimer J.; and Presnell, John G., Jr.: Supersonic Panel Flutter Test Results for Flat Fiber-Glass Sandwich Panels With Foamed Cores. NASA TN D-827, 1961.

14. Bohon, Herman L.; and Dixon, Sidney C.: Some Recent Developments in Flutter of Flat Panels. J. Aircraft, vol. 1, no. 5, Sept.-Oct. 1964, pp. 280-288.

15. Movchan, A. A.: On the Stability of a Panel Moving in a Gas. (Ob Ustoichivosti Paneli, Dvizhushcheisia v Gaze.) NASA RE 11-21-58W, 1959.

16. Stroud, W. Jefferson: The Elastic Constants for Bending and Twisting of Corrugation-Stiffened Panels. NASA TR R-166, 1963.

17. Timoshenko, S.: Strength of Materials. Part I – Elementary Theory and Problems. Second Ed., D. Van Nostrand Co., Inc., 1940, p. 308.

TABLE I.- DIMENSIONS AND STIFFNESSES OF CORRUGATION-STIFFENED PANELS

See Errata

Panel	w		d		t_1		t_2		S		$\bar{S}$		r		$\bar{r}$		γ		Material	D_s		$\frac{a}{b}$	$\frac{D_x}{D_s}$	$\frac{D_{xy}}{D_s}$
	in.	cm	in.	cm	in.	cm	in.	cm	in.	cm	in.	cm	in.	cm	in.	cm	in.	cm		in-lb	m-N			
Free-edge panels																								
U-1	1.00	2.54	0.24	0.610	0.010	0.025	0.010	0.025	----	----	0.50	1.27	-----	-----	0.25	0.635	0.13	0.33	2024-T3 aluminum alloy	0.975	0.1101	1.00	1.049	524.3
U-2	1.00	2.54	.37	.940	.011	.028	.011	.028	----	----	.50	1.27	-----	-----	.25	.635	.13	.33	Inconel X	3.893	.4399	1.00	1.496	996.0
V-1	.50	1.27	.48	1.219	.020	.051	.019	.048	----	----	----	----	0.062	0.157	.062	.157	----	----	2024-T3 aluminum alloy	7.800	.8813	1.00	1.379	457.0
V-2	1.00	2.54	.55	1.397	.011	.028	.011	.028	----	----	----	----	.062	.157	.062	.157	----	----	Inconel X	3.893	.4399	1.00	1.961	2321
V-3	1.00	2.54	.55	1.397	.010	.025	.010	.025	----	----	----	----	.062	.157	.062	.157	----	----	301 stainless steel	2.925	.3305	1.00	1.961	2771
V-4	.75	1.905	.48	1.219	.018	.046	.018	.046	----	----	----	----	.125	.318	.125	.318	----	----	Inconel X	17.059	1.9274	1.00	1.135	687.7
V-5	.75	1.905	.48	1.219	.020	.051	.020	.051	----	----	----	----	.125	.318	.125	.318	----	----	2024-T3 aluminum alloy	7.800	.8813	1.00	1.135	573.3
V-6	.50	1.27	.48	1.219	.019	.048	.019	.048	----	----	----	----	.062	.157	.062	.157	----	----	17-7 PH stainless steel	20.063	2.2668	1.00	1.138	521.0
H-1	1.00	2.54	.49	1.245	.010	.025	.010	.025	0.50	1.27	.50	1.27	-----	-----	-----	-----	.13	.33	Inconel X	2.925	.3305	1.00	1.058	2180.6
Crushed-edge panels																								
S-1	1.50	3.810	0.515	1.308	0.010	0.025	0.010	0.025	----	----	----	----	0.262	0.665	0.262	0.665	----	----	M-252 nickel base alloy	2.944	0.3326	1.54	1.844	2741
S-2	2.30	5.842	.74	1.880	.010	.025	.010	.025	----	----	----	----	.375	.953	.375	.953	----	----	M-252 nickel base alloy	2.944	.3326	1.54	1.937	5497
S-3	2.64	6.706	.74	1.880	.010	.025	.010	.025	----	----	----	----	.375	.953	.375	.953	----	----	M-252 nickel base alloy	2.944	.3326	1.54	1.933	5628
S-4	3.12	7.925	.74	1.880	.010	.025	.010	.025	----	----	----	----	.375	.953	.375	.953	----	----	M-252 nickel base alloy	2.944	.3326	1.54	1.971	5753
S-5	1.19	3.023	.515	1.308	.010	.025	.010	.025	----	----	----	----	.262	.665	.262	.665	----	----	M-252 nickel base alloy	2.944	.3326	1.54	1.747	2557
S-6	1.19	3.023	.515	1.308	.010	.025	.010	.025	----	----	----	----	.262	.665	.262	.665	----	----	2024-T3 aluminum alloy	.981	.1108	1.54	1.747	2557
S-7	1.50	3.810	.515	1.308	.010	.025	.010	.025	----	----	----	----	.262	.665	.262	.665	----	----	2024-T3 aluminum alloy	.981	.1108	1.54	1.844	2741
S-8	1.50	3.810	.74	1.880	.010	.025	.010	.025	----	----	----	----	.375	.953	.375	.953	----	----	M-252 nickel base alloy	2.944	.3326	1.54	1.649	4733
S-9	1.50	3.810	.74	1.880	.010	.025	.010	.025	----	----	----	----	.375	.953	.375	.953	----	----	2024-T3 aluminum alloy	.981	.1108	1.54	1.649	4733
S-10	1.50	3.810	.742	1.885	.008	.020	.008	.020	----	----	----	----	.375	.953	.375	.953	----	----	M-252 nickel base alloy	1.507	.1703	1.54	1.649	7397

TABLE II.- DIMENSIONS OF FLAT UNSTIFFENED FLUTTER PANELS

Panel	a		b		t		Number of bays (width b)	Material
	in.	cm	in.	cm	in.	cm		
Multi-bay panels								
1	37.20	94.49	6.00	15.24	0.0160	0.0406	3	2024-T3 aluminum alloy
2	37.20	94.49	6.00	15.24	.0403	.1024	3	2024-T3 aluminum alloy
3	37.20	94.49	3.62	9.19	.0392	.0996	5	2024-T3 aluminum alloy
4	37.20	94.49	3.62	9.19	.0325	.0826	5	2024-T3 aluminum alloy
Single-bay panels								
5	37.12	94.28	24.12	61.26	0.1250	0.3180	1	2024-T3 aluminum alloy
6	24.00	60.96	24.12	61.26	.0190	.0480	1	17-7 PH stainless steel

TABLE III.- FLUTTER DATA FOR CORRUGATION-STIFFENED PANELS

Panel	Mach number	Minimum flutter q		Δp at flutter	
		psf	kN/m^2	psf	kN/m^2
		Free-edge panels			
U-1	2.83	238	11.40	0	0
U-2	1.63	209	10.01	0	0
U-2	1.84	210	10.05	50	2.39
U-2	1.96	183	8.76	78	3.73
U-2	2.36	298	14.27	25	1.20
U-2	2.62	421	20.16	40	1.92
U-2	2.83	509	24.37	30	1.44
U-2	3.00	3400*	162.86	≈0	0
V-1	1.63	514	24.61	0	0
V-2	1.63	540	25.86	-5	-.24
V-2	1.84	580	27.77	5	.24
V-2	1.96	585	28.01	-5	-.24
V-3	1.63	294	14.08	18	.86
V-3	1.72	242	11.59	5	.24
V-3	1.84	272	13.02	15	.72
V-4	1.63	1512	72.39	0	0
V-5	1.63	296	14.17	5	.24
V-5	1.84	462	22.12	-5	-.24
V-5	1.96	512	24.51	-6	-.29
V-6	1.63	1172	56.12	72	3.45
V-6	1.84	1552	74.31	110	5.27
V-6	1.96	1848	88.48	30	1.44
H-1	1.63	253	12.11	50	2.4
H-1	1.84	504	24.13	20	.96
H-1	3.00	2900*	138.85	≈0	≈0
		Crushed-edge panels			
S-1	1.57	386	18.48	≈0	≈0
S-1	1.85	525	25.14		
S-1	2.10	678	32.46		
S-2	1.57	445	21.31		
S-2	1.85	656	31.41		
S-3	1.85	1115	53.39		
S-3	2.10	1450	69.43		
S-4	1.57	1040	49.80		
S-4	1.85	860	41.18		
S-4	2.10	1075	51.47		
S-5	2.10	905	43.33		
S-6	2.10	326	15.61		
S-7	1.57	352	16.85		
S-8	2.10	960	45.96		
S-9	2.10	135	6.46		
S-10	1.57	670	32.08		

*From reference 8.

TABLE IV.- FLUTTER DATA FOR FLAT UNSTIFFENED PANELS

Panel	M	Dynamic pressure, q		Pressure differential, Δp		Flutter motion and comments
		psf	kN/m^2	psf	kN/m^2	
Multi-bay panels						
1	2.10	318	1.523	14	0.067	
	2.10	366	1.752	12	.057	
	2.10	417	1.997	10	.048	
	2.10	467	2.236	6	.029	
	2.10	517	2.475	4	.019	
	2.10	566	2.710	1	.005	
	2.10	244	1.168	9	.043	Increase stagnation temperature 50° F (28° K)
	2.10	147	.704	6	.029	Increase stagnation temperature 50° F (28° K)
	1.86	163	.780	2	.010	
	1.86	355	1.700	4	.019	
	1.86	467	2.236	6	.029	
	1.86	555	2.657	12	.057	
	1.57	182	.871	9	.043	
2	2.10	560	2.681	17	.081	
	2.10	585	2.801	37	.177	No flutter
	2.10	500	2.394	10	.048	
	2.10	800	3.830	10	.048	Large amplitude motion initiated
	2.10	1254	6.004	70	.316	
	2.10	451	2.159	≈0	-----	
	2.10	709	3.395	≈0	-----	Large amplitude motion initiated
	1.70	822	3.936	≈0	-----	
	1.70	1283	6.143	≈0	-----	Large amplitude motion initiated
3	2.10	1020	4.884	160	.766	
	2.10	884	4.233	400	1.915	No flutter
4	2.10	1013	4.850	190	.910	Large amplitude motion initiated
Single-bay panels						
5	1.87	1580	7.565	≈0	≈0	
	1.57	1867	8.939	≈0	≈0	
6	1.87	1400	6.703	≈0	≈0	
	1.87	1790	8.571	≈0	≈0	Failure of panel

NASA-Langley, 1966 1-1541

"The aeronautical and space activities of the United States shall be conducted so as to contribute . . . to the expansion of human knowledge of phenomena in the atmosphere and space. The Administration shall provide for the widest practicable and appropriate dissemination of information concerning its activities and the results thereof."

—NATIONAL AERONAUTICS AND SPACE ACT OF 1958

NASA SCIENTIFIC AND TECHNICAL PUBLICATIONS

TECHNICAL REPORTS: Scientific and technical information considered important, complete, and a lasting contribution to existing knowledge.

TECHNICAL NOTES: Information less broad in scope but nevertheless of importance as a contribution to existing knowledge.

TECHNICAL MEMORANDUMS: Information receiving limited distribution because of preliminary data, security classification, or other reasons.

CONTRACTOR REPORTS: Technical information generated in connection with a NASA contract or grant and released under NASA auspices.

TECHNICAL TRANSLATIONS: Information published in a foreign language considered to merit NASA distribution in English.

TECHNICAL REPRINTS: Information derived from NASA activities and initially published in the form of journal articles.

SPECIAL PUBLICATIONS: Information derived from or of value to NASA activities but not necessarily reporting the results of individual NASA-programmed scientific efforts. Publications include conference proceedings, monographs, data compilations, handbooks, sourcebooks, and special bibliographies.

Details on the availability of these publications may be obtained from:

SCIENTIFIC AND TECHNICAL INFORMATION DIVISION

NATIONAL AERONAUTICS AND SPACE ADMINISTRATION

Washington, D.C. 20546